Supporting Information for

# Polarizable Additive with Intermediate Chelation Strength for Stable Aqueous Zinc-Ion Batteries

Yuting Xia[1], Rongao Tong[1], Jingxi Zhang[1], Mingjie Xu[2], Gang Shao[2], Hailong Wang[2], Yanhao Dong[1,*], Chang-An Wang[1,*]

[1]State Key Lab of New Ceramics and Fine Processing, School of Materials Science and Engineering, Tsinghua University, Beijing 100084, People's Republic of China

[2]School of Materials Science and Engineering, Zhengzhou University, Zhengzhou, Henan 450001, People's Republic of China

*Corresponding authors. E-mail: dongyanhao@tsinghua.edu.cn (Yanhao Dong); wangca@tsinghua.edu.cn (Chang-An Wang)

## Supplementary Figures and Tables

**Table S1** Stability Constants of Zinc ion-Coordination Compounds (25 ℃, the number of ligand is 1) [S1]

| Ligand | lgβ |
|---|---|
| DOTA | 19.7 |
| DTPA | 18.2 |
| EDTA | 16.3 |
| NTA | 10.7 |
| Lactic acid | 6.85 |
| Oxalic acid | 1.5 |

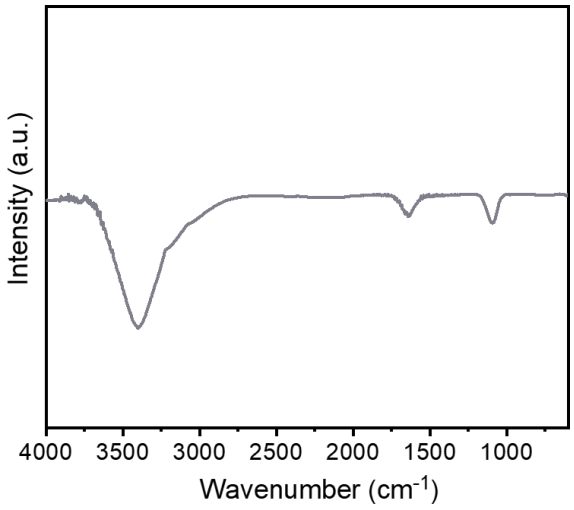


**Fig. S1** FT-IR spectra of 2M $ZnSO_4$ electrolyte

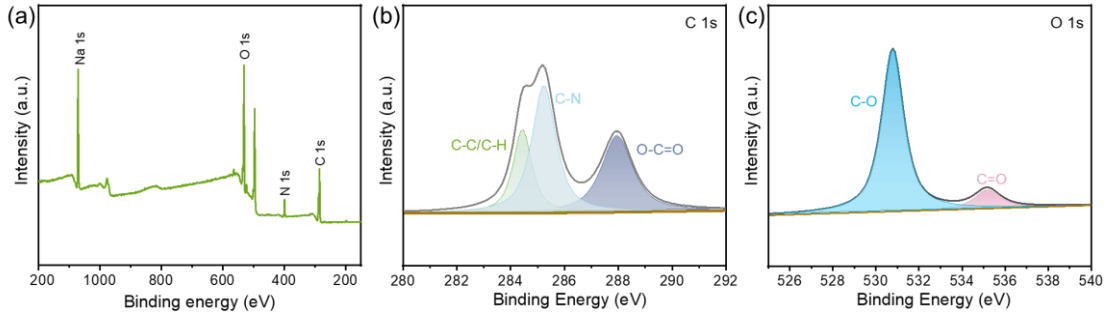


**Fig. S2** XPS spectra of the DTPA-Na powder: **a** survey scan, **b** C 1s and **c** O 1s

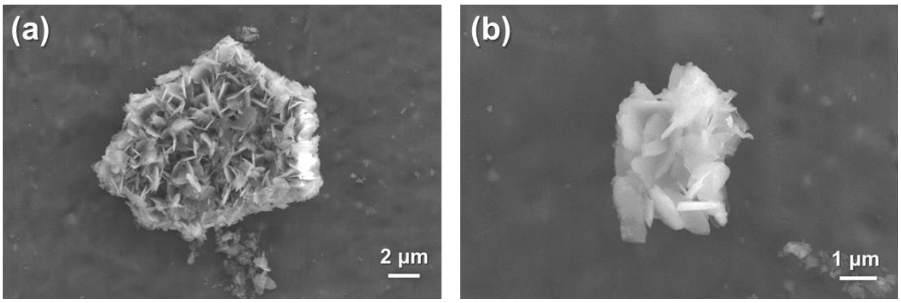


**Fig. S3** SEM images of the precipitates in the electrolyte with 2.3 wt% DTPA-Na

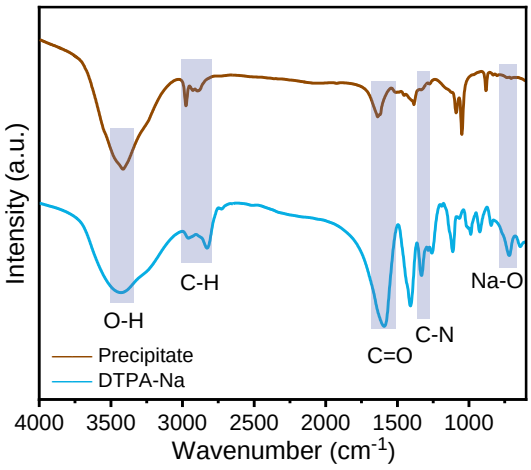


**Fig. S4** FT-IR spectra of the precipitates in the electrolyte with 2.3 wt% DTPA-Na

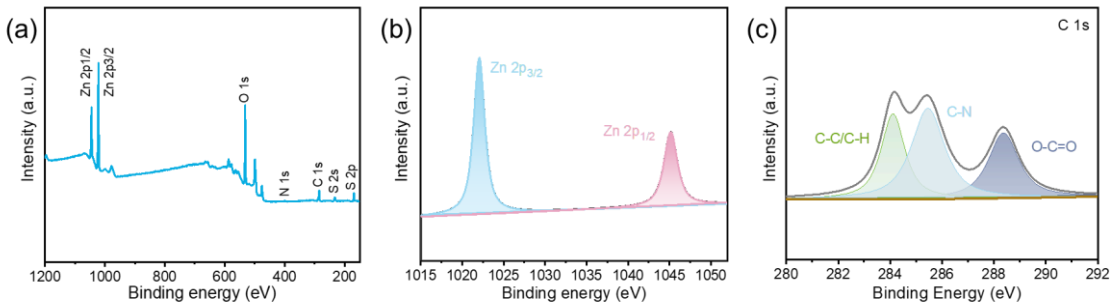


**Fig. S5** XPS spectra of the precipitates: **a** survey scan, **b** Zn 2p, **c** C 1s

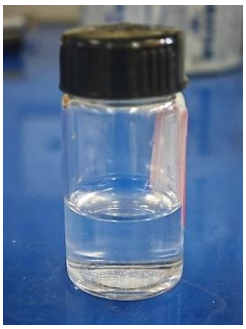

**Fig. S6** Digital photographs of the precipitates in the electrolyte with 2.3 wt% DTPA-Na

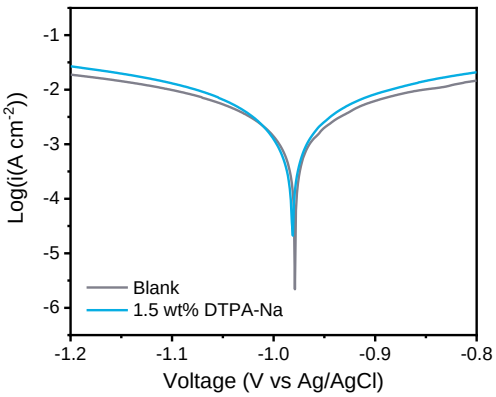


**Fig. S7** Linear polarization curves showing the corrosion on Zn foils

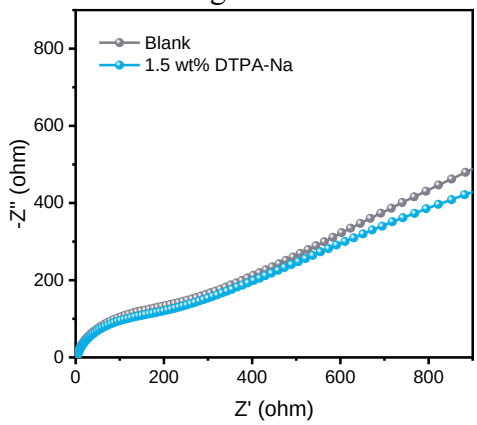


**Fig. S8** Nyquist plots of the Zn||Zn symmetric cells in the electrolytes with and without DTPA-Na addition

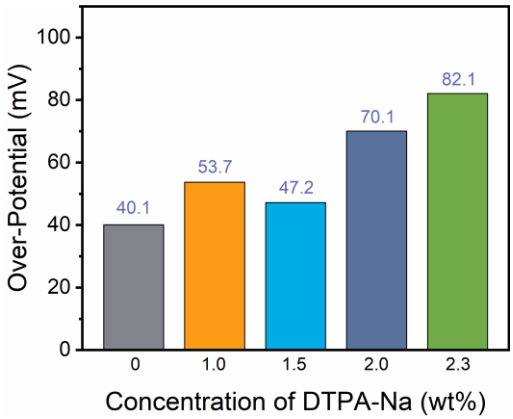


**Fig. S9** Over-potentials of symmetric cells during the 20$^{th}$ cycle with different concentrations of DTPA-Na in the electrolyte

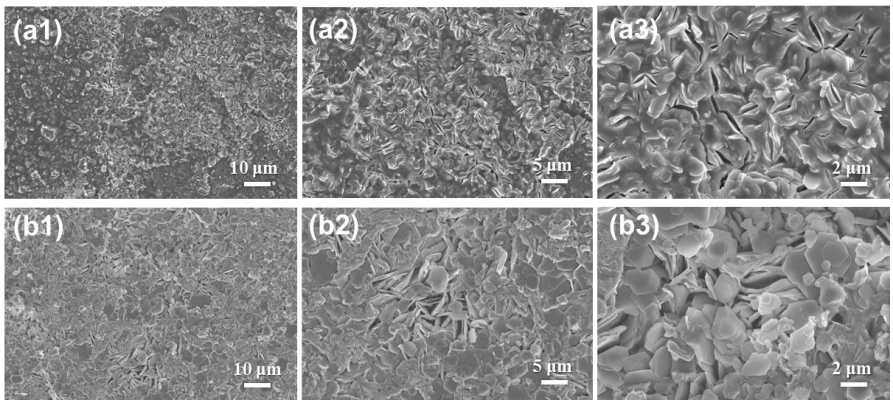


**Fig. S10** Surface morphology of Zn foils after 100 cycles in Zn||Zn symmetric coin cells with **a** the blank electrolyte and **b** the designed electrolyte

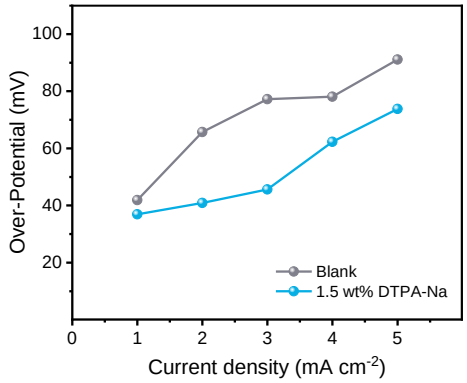


**Fig. S11** Over-potentials of Zn||Zn symmetric cells at current densities from 1 to 5 mA $cm^{-1}$

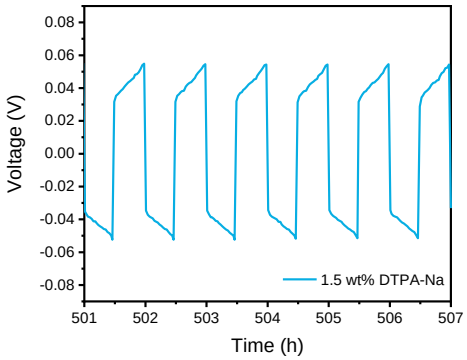


**Fig. S12** Voltage-time profiles comparison of Zn||Zn symmetric cells at 2 mA $cm^{-2}$ and 1 mAh $cm^{-2}$ for the selected cycles

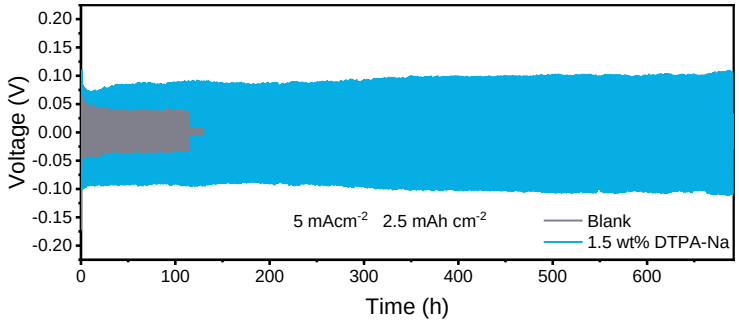


**Fig. S13** Long cycle performance of symmetric cells at 5 mA $cm^{-2}$ and 2.5 mAh $cm^{-2}$

**Table S2** Comparisons of cycling performance of the designed electrolytes in symmetrical batteries with some reported modified anodes for AZIBs

| No. | Electrolyte Component | Current Density (mA $cm^{-2}$) | Areal Capacity (mAh $cm^{-2}$) | Cycling Duration (h) | References |
|---|---|---|---|---|---|
| 1 | 2 M $ZnSO_4$ + 1.5 wt% DTPA-Na | 1<br>2<br>5 | 0.5<br>1<br>2.5 | 3500<br>800<br>450 | **This work** |
| 2 | 2 M $ZnSO_4$ + 0.0085 m $La(NO_3)_3$ | 1 | 1 | 1200 | [S2] |
| 3 | 2 M $ZnSO_4$ + 75 × $10^{-3}$ m $Na_4EDTA$ | 2<br>5 | 2<br>2 | 450<br>2000 | [S3] |
| 4 | 2 M $ZnSO_4$ + 8 mg $mL^{-1}$ PASP | 0.5<br>20 | 0.5<br>1 | 3200<br>200 | [S4] |
| 5 | 2 M $ZnSO_4$ + 1 vol% DM | 2 | 2 | 400 | [S5] |
| 6 | 2 M $ZnSO_4$ + 0.2 M $MnSO_4$ + 1% $Et_2O$ + 30% EG | 0.5<br>5 | 0.5<br>5 | 700<br>700 | [S6] |
| 7 | 2 M $ZnSO_4$ + 0.5 g $L^{-1}$ TMBAC | 2<br>10 | 2<br>5 | 900<br>470 | [S7] |
| 8 | 2 M $ZnSO_4$ + 0.5 g $L^{-1}$ Sac | 10 | 10 | 600 | [S8] |
| 9 | 1 M $ZnSO_4$ + 5% 1,4-Dioxane | 5 | 2.5 | 600 | [S9] |
| 10 | 1 M $ZnSO_4$ + 10 vol% PG | 2 | 2 | 1000 | [S10] |
| 11 | 3 m $ZnAc_2$ + 30 m KAc + 3 m LiAc | 0.1 | 0.2 | 1000 | [S11] |
| 12 | 4 M $Zn(CF_3SO_3)_2$ + 0.5 M $Me_3EtNOTF$ | 0.5 | 0.25 | 6000 | [S12] |
| 13 | 1.3 m $ZnCl_2/H_2O$–DMSO (volume ratio of $H_2O$/DMSO = 4.3:1) | 0.5 | 0.5 | 1000 | [S13] |
| 14 | 30 m $ZnCl_2$ | 0.2 | 0.03 | 600 | [S14] |
| 15 | 3 m $Zn(OTf)_2$ + 17 m $NaClO_4$ | 1 | 0.25 | 1600 | [S15] |

**Fig. S14** Symmetrical cells assembled in transparent H-type tanks

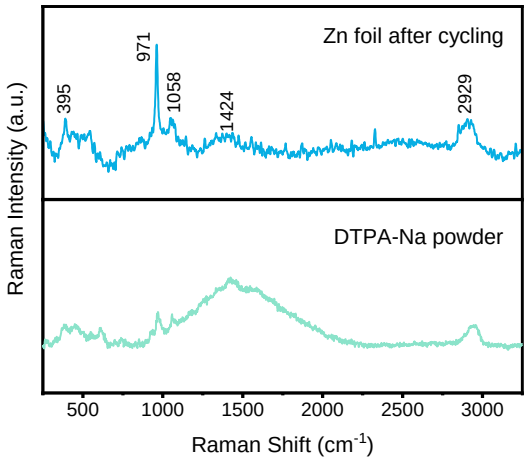


**Fig. S15** Raman spectroscopies of the surface of the Zn foils after 100 cycles in Zn||Zn symmetric coin cells with the designed electrolyte

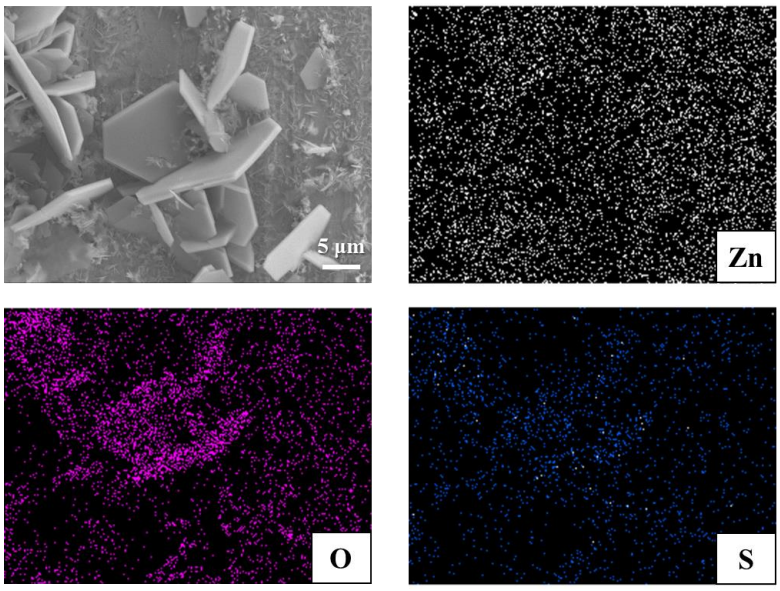


**Fig. S16** Surface morphology and corresponding EDS element mapping of Zn, O, and S of the Zn foil immersed in 2M $ZnSO_4$ electrolyte for one month

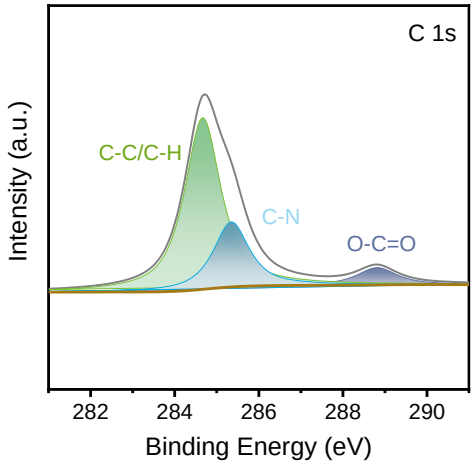


**Fig. S17** XPS high-resolution for C 1s of the Zn foil after immersed in the electrolyte with 1.5 wt% DTPA-Na for one month

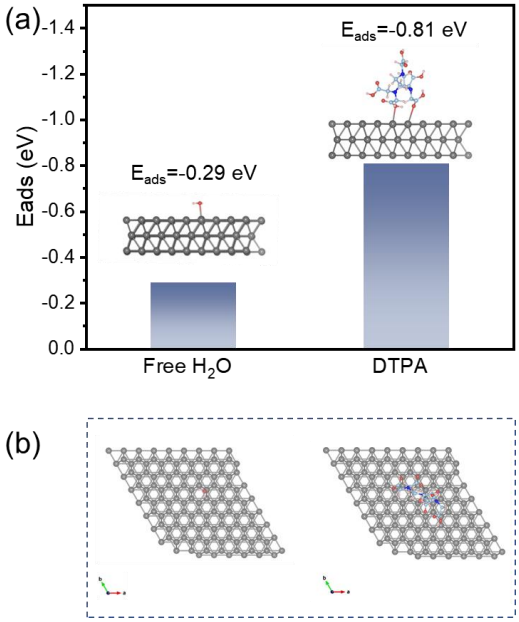


**Fig. S18** Adsorbed models of free $H_2O$ and DTPA on Zn (002) surface and corresponding adsorption energy

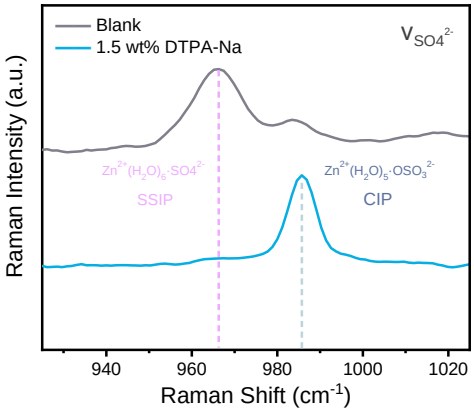


**Fig. S19** Raman spectroscopies of the surface of the Zn foils after immersed in different electrolytes for one month

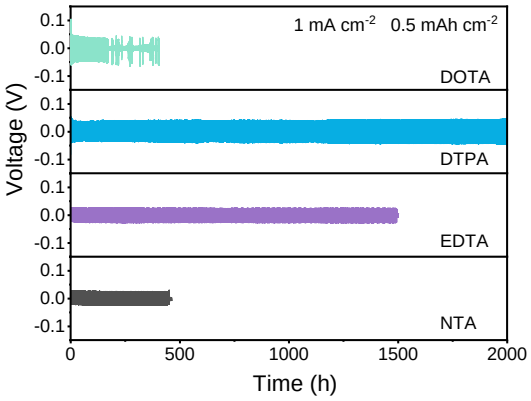


**Fig. S20** Long cycle performance of symmetric cells assembled with different ligands at 1 mA $cm^{-2}$ and 0.5 mAh $cm^{-2}$

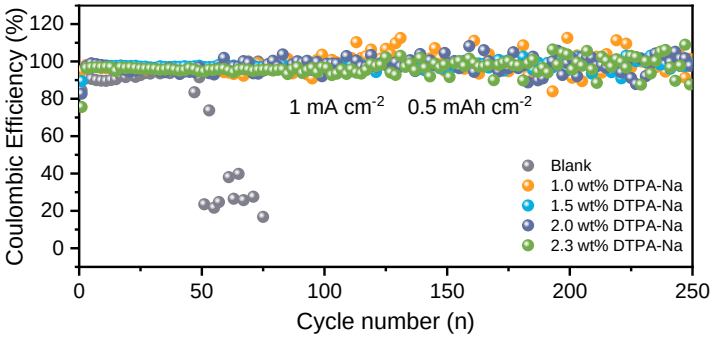


**Fig. S21** Coulombic efficiency of Zn plating/stripping on Ti foils in the different electrolytes at 1 mA $cm^{-2}$ with 0.5 mAh $cm^{-2}$

**Table S3** The average CE of Zn||Ti half cells in the electrolytes with different concentrations of DTPA-Na after 250 cycles

| **Electrolyte component** | **Average CE (%)** |
|---|---|
| Blank | 92.4 (40 cycles) |
| 1.0 wt% DTPA-Na | 97.4 |
| **1.5 wt% DTPA-Na** | **97.8** |
| 2.0 wt% DTPA-Na | 97.4 |
| 2.3 wt% DTPA-Na | 96.9 |

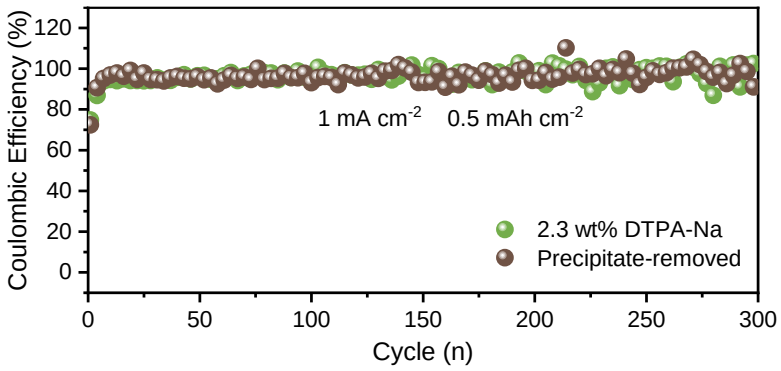


**Fig. S22** Coulombic efficiency of the Zn||Ti half cell with/without precipitates in electrolyte

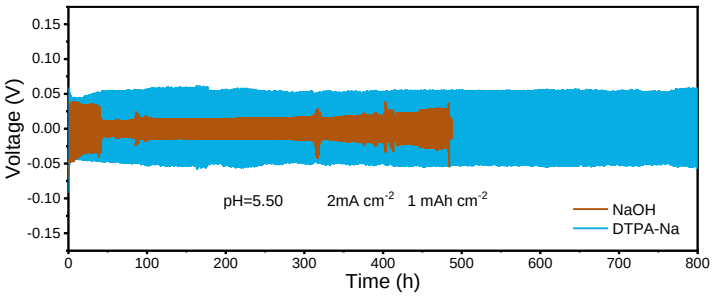


**Fig. S23** Long cycle performance of symmetric cells in the electrolytes with pH of 5.50

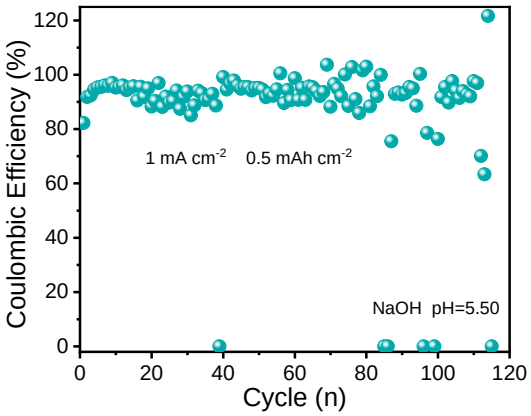


**Fig. S24** Coulombic efficiency of Zn plating/stripping on Ti foil in the electrolyte with pH of 5.50 adjusted by NaOH

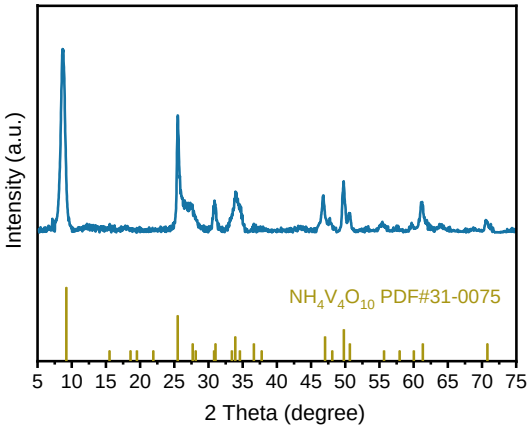


**Fig. S25** XRD pattern of the prepared $NH_4V_4O_{10}$ cathode active materials

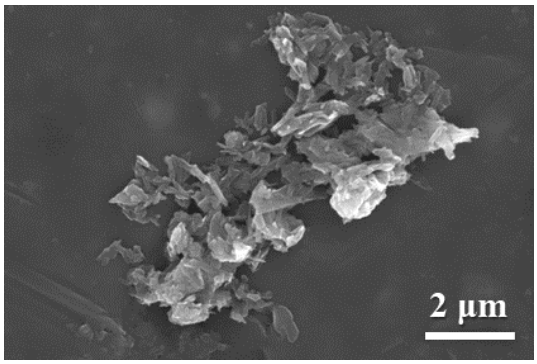


**Fig. S26** SEM image of the prepared $NH_4V_4O_{10}$ cathode active materials

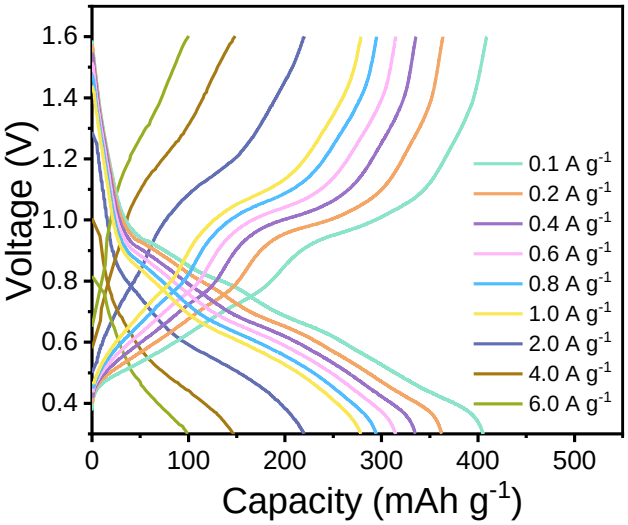


**Fig. S27** Discharge/charge profiles of Zn||$NH_4V_4O_{10}$ cells at different current density

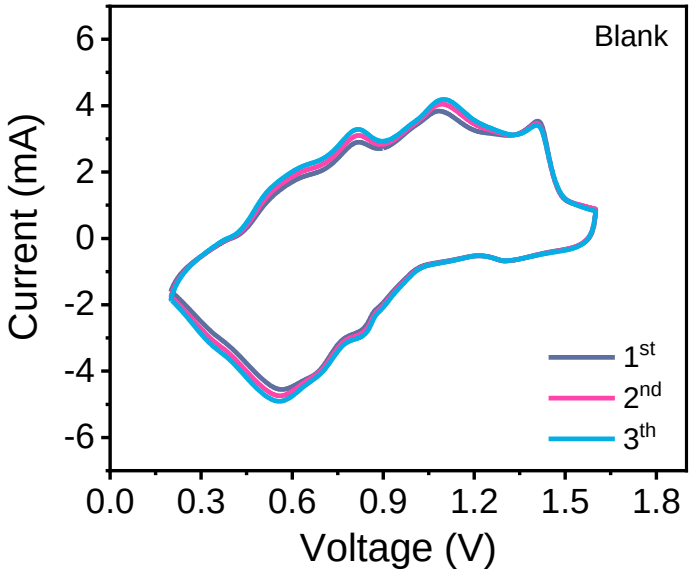


**Fig. S28** CV profiles of Zn||$NH_4V_4O_{10}$ cell in the baseline electrolyte at 0.1 mV $s^{-1}$

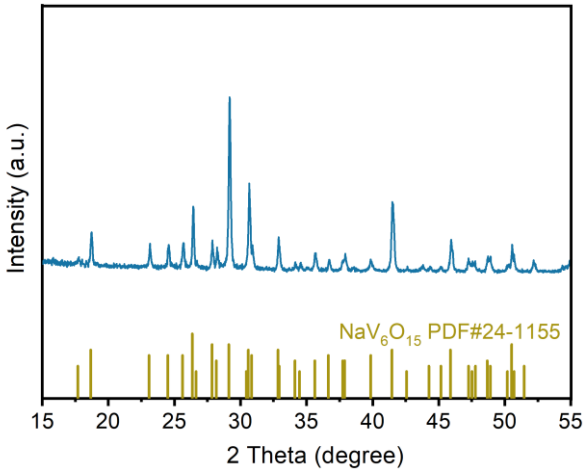


**Fig. S29** XRD pattern of the prepared $NaV_6O_{15}$ cathode active materials

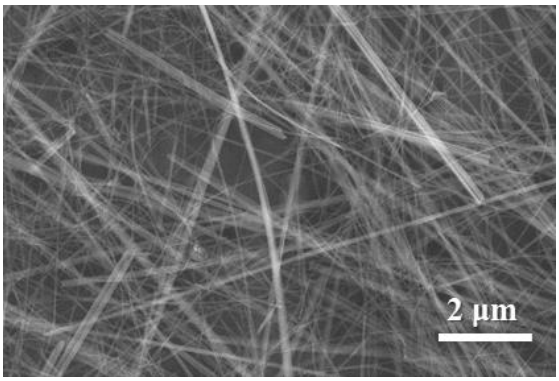


**Fig. S30** SEM image of the prepared $NaV_6O_{15}$ cathode active materials

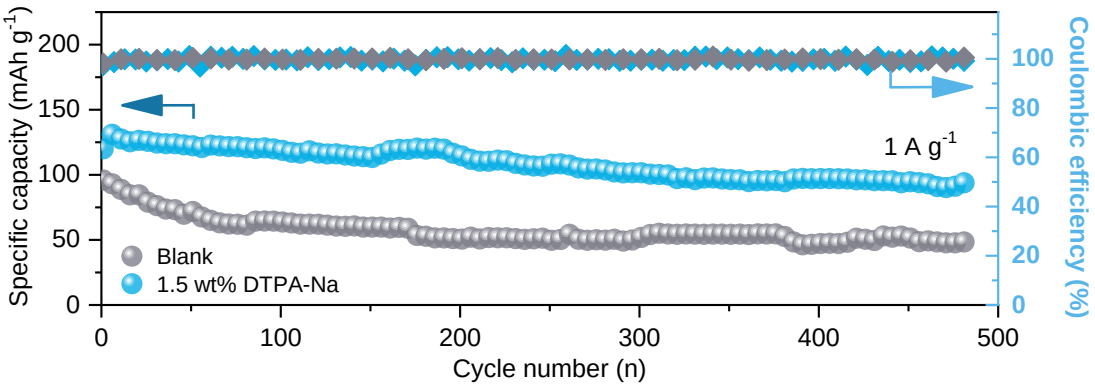


**Fig. S31** Cycle performance Zn||$NaV_6O_{15}$ cells at 1 A $g^{-1}$

## Supplementary References

[S1] NIST standard reference database 46. http://www.nist.gov/srd/nist46.cfm

[S2] R. Zhao, H. Wang, H. Du, Y. Yang, Z. Gao et al., Lanthanum nitrate as aqueous electrolyte additive for favourable zinc metal electrodeposition. Nat. Commun. **13**, 3252 (2022). https://doi.org/10.1038/s41467-022-30939-8

[S3] S.-J. Zhang, J. Hao, D. Luo, P.-F. Zhang, B. Zhang et al., Dual-function electrolyte additive for highly reversible Zn anode. Adv. Energy Mater. **11**, 2102010 (2021). https://doi.org/10.1002/aenm.202102010

[S4] T. Zhou, Y. Mu, L. Chen, D. Li, W. Liu et al., Toward stable zinc aqueous rechargeable batteries by anode morphology modulation via polyaspartic acid additive. Energy Storage Mater. **45**, 777–785 (2022). https://doi.org/10.1016/j.ensm.2021.12.028

[S5] J. Cui, X. Liu, Y. Xie, K. Wu, Y. Wang et al., Improved electrochemical reversibility of Zn plating/stripping: a promising approach to suppress water-induced issues through the formation of H-bonding. Mater. Today Energy **18**, 100563 (2020). https://doi.org/10.1016/j.mtener.2020.100563

[S6] A. Wang, W. Zhou, A. Huang, M. Chen, Q. Tian et al., Developing improved electrolytes for aqueous zinc-ion batteries to achieve excellent cyclability and

antifreezing ability. J. Colloid Interface Sci. **586**, 362–370 (2021). https://doi.org/10.1016/j.jcis.2020.10.099

[S7] K. Guan, L. Tao, R. Yang, H. Zhang, N. Wang et al., Anti-corrosion for reversible zinc anode via a hydrophobic interface in aqueous zinc batteries (adv. energy mater. 9/2022). Adv. Energy Mater. **12**, 2270037 (2022). https://doi.org/10.1002/aenm.202270037

[S8] C. Huang, X. Zhao, S. Liu, Y. Hao, Q. Tang et al., Stabilizing zinc anodes by regulating the electrical double layer with saccharin anions. Adv. Mater. **33**, e2100445 (2021). https://doi.org/10.1002/adma.202100445

[S9] R. Feng, X. Chi, Q. Qiu, J. Wu, J. Huang et al., Cyclic ether-water hybrid electrolyte-guided dendrite-free lamellar zinc deposition by tuning the solvation structure for high-performance aqueous zinc-ion batteries. ACS Appl. Mater. Interfaces **13**, 40638–40647 (2021). https://doi.org/10.1021/acsami.1c11106

[S10] Y. Shang, P. Kumar, T. Musso, U. Mittal, Q. Du et al., Long-life Zn anode enabled by low volume concentration of a benign electrolyte additive. Adv. Funct. Mater. **32**, 2200606 (2022). https://doi.org/10.1002/adfm.202200606

[S11] J. Han, A. Mariani, A. Varzi, S. Passerini, Green and low-cost acetate-based electrolytes for the highly reversible zinc anode. J. Power Sources **485**, 229329 (2021). https://doi.org/10.1016/j.jpowsour.2020.229329

[S12] L. Cao, D. Li, T. Pollard, T. Deng, B. Zhang et al., Fluorinated interphase enables reversible aqueous zinc battery chemistries. Nat. Nanotechnol. **16**, 902–910 (2021). https://doi.org/10.1038/s41565-021-00905-4

[S13] L. Cao, D. Li, E. Hu, J. Xu, T. Deng et al., Solvation structure design for aqueous Zn metal batteries. J. Am. Chem. Soc. **142**, 21404–21409 (2020). https://doi.org/10.1021/jacs.0c09794

[S14] C. Zhang, J. Holoubek, X. Wu, A. Daniyar, L. Zhu et al., A $ZnCl_2$ water-in-salt electrolyte for a reversible Zn metal anode. Chem. Commun. **54**, 14097–14099 (2018). https://doi.org/10.1039/C8CC07730D

[S15] H. Ao, W. Zhu, M. Liu, W. Zhang, Z. Hou et al., High-voltage and super-stable aqueous sodium-zinc hybrid ion batteries enabled by double solvation structures in concentrated electrolyte. Small Methods **5**, e2100418 (2021). https://doi.org/10.1002/smtd.202100418